RSC Applied Polymers

PAPER

View Article Online
View Journal

Cite this: DOI: 10.1039/d5lp00413f

Systematic investigation of urea containing sidechains in electrochromic ProDOT and EDOT copolymers

Md Mahmudul Hasan,[a] Raul S. Ramos,[a] Kavish Saini,[a] Md Shahjahan Mahmud,[b] Ashley Morales,[a] Adrian Bocanegra Richarte,[a] Michael Lyubchenko,[c] Sreeprasad T. Sreenivasan, [a] Yirong Lin[b] and Robert M. Pankow *[a]

Strategies for the sidechain engineering of conjugated polymers have advanced to include H-bonding functional groups, such as amides, carbamates, and amino acid derivatives, enabling new capabilities in emerging organic electronic device technologies. However, this has been limited to secondary amides and carbamates with limited examples of urea functional groups. Here, the systematic investigation of both the alkyl substituent and the inclusion of a H-bonding urea functional group is reported for a series of 3,4-propylenedioxythiophene (ProDOT) and 3,4-ethylenedioxythiophene (EDOT) copolymers to determine how both modification of the alkyl substituent on ProDOT [hexyloxy (C6) or decyloxy (C10)] and the functional group on EDOT [phthalimide (Ph) or urea (Ur)] alters the optical, electrochemical, and electrochromic properties. The polymers (PC6-Ph, PC6-Ur, PC10-Ph, and PC10-Ur) were synthesized *via* direct arylation polymerization, and fully characterized *via* ATR-FTIR, high-temperature NMR, MALDI-TOF, DSC, TGA, AFM, and SEM. ATR-FTIR, NMR, and MALDI-TOF revealed the desired functional groups were retained in the polymer. It was found that the optical and electrochemical properties showed a greater dependence on the pendant substituent identity (phthalimide or urea) rather than the alkyl substituent. Electrochromic characterization revealed a dependence on both the alkyl substituent and functional group identity where proper pairing could yield a 50% reduction in switching time and desirable coloration efficiencies (up to 93 $cm^2\ C^{-1}$). Overall, these findings provide a comprehensive analysis of both the role of the alkyl substituent identity and the inclusion of a urea functional group guiding the future molecular design of electrochromic polymers.

Received 30th December 2025,
Accepted 11th March 2026

DOI: 10.1039/d5lp00413f

rsc.li/rscapplpolym

Introduction

Sidechain engineering is an effective strategy for tuning the optical, electrochemical, and charge-transport properties and morphology and microstructure of conjugated polymers.[1–7] This aspect of molecular design includes modification of the sidechain identity from typical linear or branched alkyls to sidechains with heteroatoms or various functional groups enabling sustainable solvent processing, compatibility with aqueous electrolytes, or opportunities for post-polymerization functionalization.[3,8–11] For example, linear alkyl sidechains when incorporated into a regioregular arrangement have been shown to promote the formation of semicrystalline domains, due to improved sidechain interdigitation and π–π interactions, while branched alkyl substituents can disrupt the formation of crystalline domains by inhibiting efficient interpolymer π–π overlap.[12,13] Additional structural considerations, such as the length of the sidechain, the location of the branching point, and the inclusion of heteroatoms can further influence polymer self-assembly and the preferential formation of polymer semicrystalline or amorphous phases.[14–16] Recently, there has been growing research interest in the inclusion of heteroatoms and various functional groups in conjugated polymers to enable new materials capabilities or optimize organic electronic device performance metrics (Fig. 1A). Specifically, the inclusion of oligo(ethylene glycol) sidechains have provided improved electrolyte penetration and exchange with aqueous electrolytes suitable for organic electrochemical transistors,[17–20] and H-bonding functional groups, such as amides and carbamates, have afforded conjugated polymers with robust mechanical properties and self-

[a]Department of Chemistry and Biochemistry, University of Texas at El Paso, El Paso, Texas 79968, USA. E-mail: rmpankow@utep.edu
[b]Department of Aerospace and Mechanical Engineering, University of Texas at El Paso, El Paso, Texas 79968, USA
[c]Department of Metallurgical, Materials and Biomedical Engineering, University of Texas at El Paso, El Paso, Texas 79968, USA

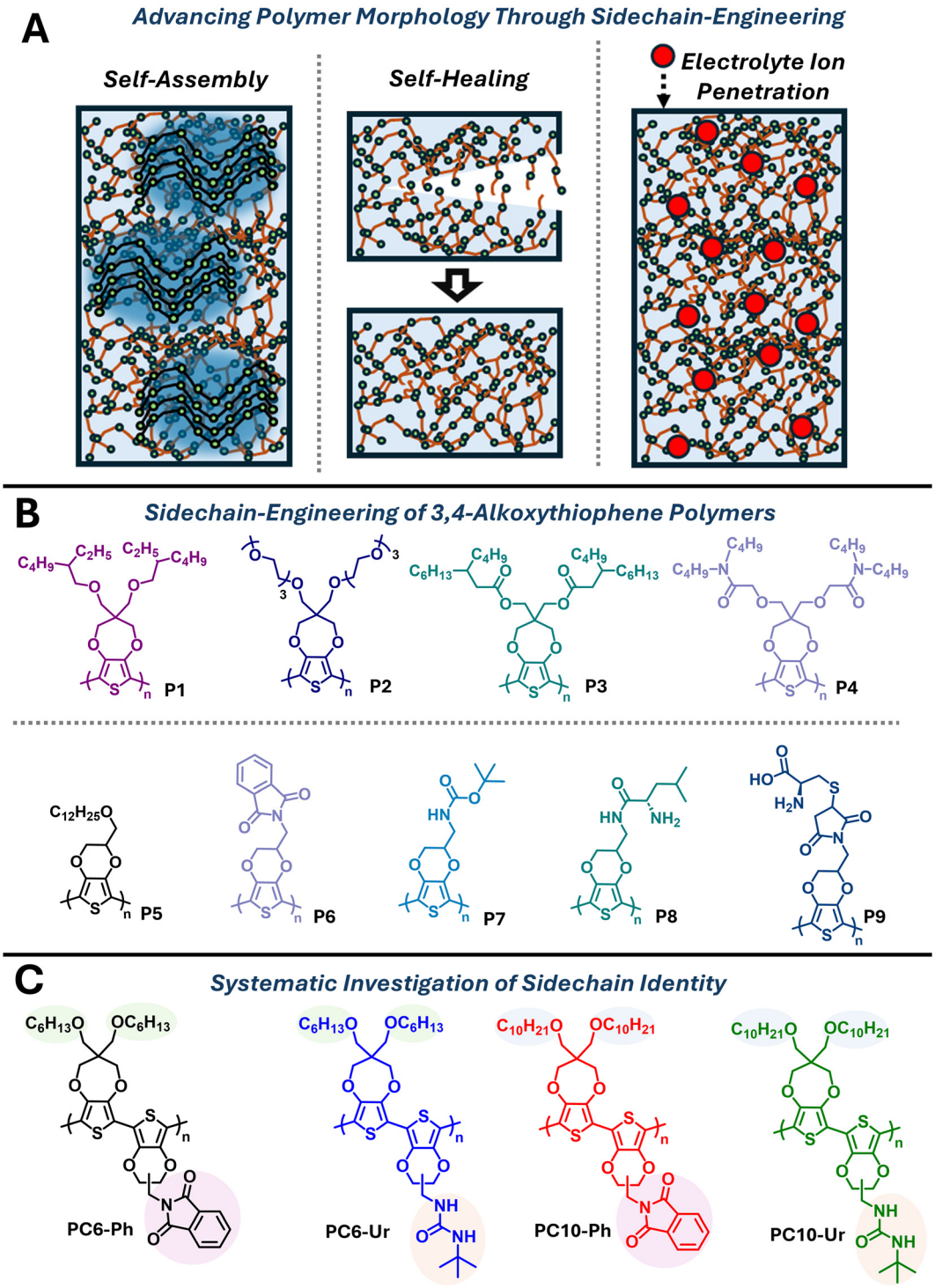

Fig. 1 (A) Depiction of notable morphological parameters controlled through polymer sidechain engineering: self-assembly, self-healing, and electrolyte ion penetration. (B) Overview of select 3,4-alkoxythiophene polymer structures highlighting strategies in conjugated polymer sidechain engineering. (C) Depiction of the polymer structures synthesized in this study.

healing capabilities where the H-bonds impart a dynamic network capable of dissipating mechanical force or resolving nanocrack formation from applied mechanical strain.[21–28]

3,4-Alkoxythiophenes, such as 3,4-ethylenedioxythiophene (EDOT) and 3,4-propylenedioxythiophene (ProDOT), are a structural class of repeat unit where sidechain engineering is prevalent, due to the widespread incorporation of EDOT and

ProDOT in numerous organic electronic technologies, including electrochromics,[29–31] photovoltaics,[32] electrochemical transistors,[33,34] and lithium-ion batteries (Fig. 1B).[35,36] The key advantages of 3,4-alkoxythiophenes imparted through the molecular design include electrochemical redox stability, due to the electron-donating alkoxy substituents in the 3,4-positions, and the ease of structural modification through the use of common building blocks with tuneable scaffolds and concise syntheses.[35] Examples include linear or branched aliphatic sidechains (P1 and P5), oligo(ethylene glycol) sidechains (P2), and those incorporating various carbonyl functionalities (P3–P9).[37–45] Of particular note are P7–P9, which incorporate carbamate sidechains capable of H-bonding (P7) or amino-acid derivatives (P8 and P9).[43–45] P7–P9 are synthesized *via* chemical or electrochemical oxidative polymerization yielding insoluble polymer products, due to the absence of solubilizing alkyl substituents, that preclude extensive structural characterization or limit solution processing capabilities. Moreover, the incorporation of H-bonding functionalities, such as amides or related derivatives, often occurs at low compositions (5–20%) to ensure solubility and processability in common organic solvents where over incorporation can lead to insoluble polymers due to extensive H-bonding.[21–23,46] Less studied H-bonding functionalities in conjugated polymers include urea, which have imparted desirable mechanical properties and self-healing capabilities in non-conjugated polymers and have provided improved charge transport properties in conjugated polymers through morphological control.[26,47,48]

Here, ProDOT and EDOT copolymers with phthalimide or urea containing functional groups are systematically investigated where the identity of the alkyl substituent on ProDOT [either hexyloxy (C6) or decyloxy (C10)] and the functional group on EDOT [phthalimide (Ph) or urea (Ur)] are modified to elucidate the effects on the polymer optical, electrochemical, and electrochromic properties (Fig. 1C). By varying the identity of the alkyl substituent and inclusion of the phthalimide or urea functional group of the polymers (PC6-Ph, PC6-Ur, PC10-Ph, and PC10-Ur), the effects of alkyl substituent elongation (C6 *versus* C10) and inclusion of H-bonding functional group (urea) can be simultaneously probed and compared to the non-H-bonding control (phthalimide). The synthesis of the urea functionalized EDOT monomer incorporates Gabriel synthesis for the synthesis of amine precursor followed by treatment with *t*-butyl isocyanate to yield the urea functional group. The polymers were synthesized *via* direct arylation polymerization (DArP), and the structures of the polymers were confirmed using ATR-FTIR spectroscopy, high-temperature ^{1}H-NMR spectroscopy, and MALDI-TOF spectrometry. Optical absorption spectroscopy and cyclic voltammetry revealed a greater dependence of the identity of the urea/phthalimide functional group rather than that of the alkyl substituent (C6 or C10). Electrochromic characterization also revealed a greater dependence on functional group identity (phthalimide or urea) where the phthalimide functional group provides comparable switching times for PC6-Ph/PC10-Ph (t_b/t_c = 6.1/10.4 and 9.7/8.1 s) and coloration efficiencies (CE = 55 and 61 cm^2 C^{-1}) while the urea functional group in PC6-Ur/PC10-Ur affords markedly different switching times (t_b/t_c = 6.4/15.4 and 6.2/8.4 s) and coloration efficiencies (CE = 93 and 25 cm^2 C^{-1}). Lastly, the polymer morphology and surface topology was probed *via* AFM and SEM revealing a smooth, featureless morphology characteristic of regiorandom polythiophenes.

Results and discussion

Monomer and polymer synthesis

Monomer and polymer synthesis are shown in Fig. 2A with detailed synthetic procedures and structural characterization (NMR, ATR-IR, and MALDI-TOF) provided in the SI (SI; see Schemes S1 and S2 and Fig. S1–S18). Briefly, **1** was substituted with phthalimide followed by bromination to yield **3**, which was then treated with hydrazine hydrate to afford **4**. Notably, **4** is typically prepared by treating **1** with sodium azide followed by reduction to yield the free amine, and so the synthetic route detailed here provides a facile, scalable alternative to access the amine *via* Gabriel synthesis.[48] Next, **4** was combined with *t*-butyl isocyanate to provide the urea functionalized EDOT monomer **5**. The *t*-butyl substituent was selected, due to its ability to limit H-bonding thereby ensuring solution processable polymers.[49] ProDOT monomers **6** and **7** were prepared following literature procedures where monomer **6** contains hexyloxy sidechains and monomer **7** contains decyloxy sidechains.[38]

The regiorandom and stereorandom polymers were then synthesized *via* direct arylation polymerization (DArP), which has been used to prepare a variety of ProDOT and EDOT copolymers.[50–52] Specifically, monomer **6** was paired with **3** or **5** to yield PC6-Ph and PC6-Ur, and **7** was paired with **3** or **5** to yield PC10-Ph and PC10-Ur. This pairing of monomers allows for the direct comparison of the alkyl substituent length [hexyloxy (C6) *versus* decyloxy (C10)] and presence of a carbonyl containing functionality capable of hydrogen bonding [urea (Ur)] or incapable of hydrogen bonding [phthalimide (Ph)]. The high-temperature (140 °C), phosphine-free conditions employed by Reynolds *et al.* were found to afford desirable polymer products in good yields (51–81%).[50,51] Other DArP conditions, such as those employing CPME and DMA solvent mixtures, were evaluated, but these did not afford any polymer products.[36] The polymers were isolated in the $CHCl_3$ Soxhlet fraction, and no insoluble material was observed in the thimble following extraction. Overall, the polymers were found to be soluble in heated chlorinated solvents, such as $CHCl_3$ and $C_2D_2Cl_4$. However, due to the incorporation of the polar phthalimide or urea groups, the solubility of oligomeric species was observed in the MeOH fraction rather than in hexanes, and the polymers had to be precipitated in hexanes rather than MeOH. Note, analysis of the molecular weight distribution was attempted using gel-permeation chromatography (GPC). However, the polymers were found to be incompatible with GPC instrumentation ($CHCl_3$ eluent at 40 °C) necessitat-

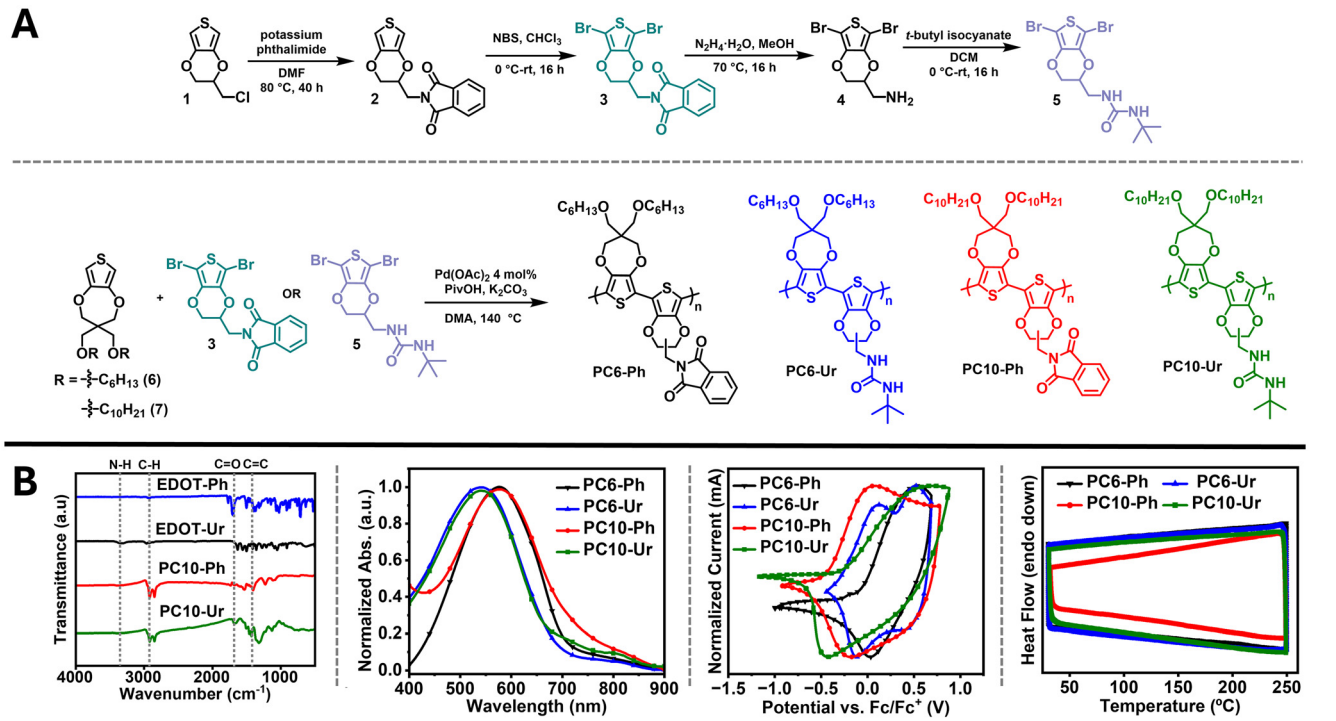

Fig. 2 (A) Monomer and polymer synthesis. (B) ATR-FTIR spectra, optical absorption spectra, cyclic voltammograms, and DSC thermograms of PC6-Ph, PC6-Ur, PC10-Ph, and PC10-Ur.

ing analysis *via* MALDI-TOF, which is detailed in a following section.

ATR-FTIR (Fig. 2B and Fig. S11 and S12) and high-temperature (80 °C in $C_2D_2Cl_4$) NMR spectroscopy (Fig. S13–S16) were used to evaluate the polymer structure. ATR-FTIR measurements show comparable spectral features corresponding to the functional groups present in the monomers and polymers (phthalimide and urea). With PC10-Ph and PC10-Ur as examples, notable features in the IR spectrum include the C═O stretches for phthalimide (1736 cm^{-1}) *versus* urea (1666 cm^{-1}) and the presence of a N–H stretch (3365 cm^{-1}) for PC10-Ur. These align well with the respective monomers where the C═O stretch for **3** (1700 cm^{-1}) and **5** (1632 cm^{-1}) occur at comparable wavenumbers, as well as the N–H stretch for **5** (3319 cm^{-1}). The chemical shifts of the resonances present in the monomer NMR spectra (Fig. S5–S10) provide alignment with the respective polymers (Fig. S13–S16) with identifiable resonances corresponding to the phthalimide (*circa* 7.90 ppm) and urea moieties (*circa* 4.50 ppm), albeit the broad, featureless resonances of the polymer NMR spectra limit the extent of analyses possible.

Contact angle measurements were performed on polymer films coated on glass-ITO substrates using DI-H_2O and ethylene glycol to assess the relative hydrophilicity (Fig. S19, SI). It was observed that the identity of the ProDOT alkyl sidechain (C6 or C10) played a predominant role in determining the hydrophilicity of the polymers where H_2O drop contact angles for PC6-Ph/PC6-Ur and PC10-Ph/PC10-Ur were found to be 82.5°/87.6° and 91.2°/95.4°, respectively. This indicates that PC10-Ph/PC10-Ur are hydrophobic, and although the water drop contact angle for PC6-Ph/PC6-Ur is considered within the hydrophilic regime ($\theta < 90°$)[53] it is well above the contact angle for PEDOT:PSS and glycolated thiophenes which are compatible with aqueous electrolytes ($\theta < 65°$).[54]

Optical absorption and cyclic voltammetry

Optical absorption measurements were performed using polymer films coated on glass substrates with the spectra provided in Fig. 2B and the corresponding data tabulated in Table 1. It was found the identity of the sidechain unit on the ProDOT comonomer (C6 or C10) has little influence on the optical absorption, where the inclusion of either the phthalimide or urea functionalized EDOT results in marked changes in the absorption profile. Specifically, PC6-Ph/PC10-Ph were found to have redshifted λ_{max} (λ_{max} = 578 nm) and comparable optical bandgaps (E_g) (1.76/1.74 eV) relative to PC6-Ur/PC10-Ur (λ_{max} = 541 nm and 1.81/1.86 eV), respectively. The optical absorption profiles for PC6-Ph/PC10-Ph and PC6-Ur/PC10-Ur align well with those reported for other ProDOT and EDOT containing copolymers.[37,50–52]

Electrochemical measurements (CV and scan rate dependence) were performed using polymer films drop-casted onto a glassy-carbon working electrode from 20 mg mL^{-1} solutions in 0.1 M $LiPF_6$/PC with a Pt-wire counter and Ag-wire psuedoreference electrode (Fig. 2B and Table 1). The polymer films were electrochemically conditioned prior to measurement (cycled 10× from −1.0 to +1.0 V) to ensure a stable polymer morphology and reproducible redox features.[52] As with the optical

Table 1 Molecular weight, thermal, optical, electrochemical, and electrochromic characterization data for PC6-Ph, PC6-Ur, PC10-Ph, and PC10-Ur

Polymer	M_n (kg mol^{-1})[a]; $Đ$[a]	T_d[b] (°C)	λ_{max} (nm); E_g[c] (eV)	E_{ox}^{onset}[d] (V)	HOMO[e] (eV)	LUMO[f] (eV)	ΔT% (%)	t_b/t_c (s)	CE (cm^2 C^{-1})
PC6-Ph	3.7; 1.05	320	578, 1.76	−0.25	−4.55	−2.79	39.8	6.1/10.4	55
PC6-Ur	3.0; 1.02	292	541, 1.81	−0.32	−4.48	−2.67	28.9	6.4/15.2	93
PC10-Ph	3.6; 1.08	300	578, 1.74	−0.26	−4.54	−2.80	27.7	9.7/8.1	61
PC10-Ur	3.2; 1.03	315	541, 1.86	−0.45	−4.25	−2.39	32.3	6.2/8.4	25

[a] Estimated *via* MALDI-TOF spectrometry following purification *via* Soxhlet extraction. [b] Measured at 5% mass loss. [c] Estimated using the equation $E_g = 1240/\lambda_{onset}$. [d] Measured using 0.1 M $LiPF_6$/PC electrolyte *versus* Fc/Fc^+. [e] Estimated using the formula $E = -E_{onset} + (-4.80\ eV)$. [f] Estimated using the formula $E_{LUMO} = E_{HOMO} + E_g$.

absorption measurements, the voltammograms show a greater dependence on identity of the EDOT sidechain functionality (Ph or Ur) rather than the sidechains of the ProDOT comonomer (C6 or C10). Specifically, PC6-Ph/PC10-Ph and PC6-Ur/PC10-Ur show comparable electrochemical oxidation onsets (E_{ox}^{onset}) (−0.25/−0.26 V and −0.32/−0.45 V) and HOMO energy levels (−4.55/−4.54 eV and −4.48/−4.25 eV). Although there is greater deviation between PC6-Ur/PC10-Ur relative to PC6-Ph/PC10-Ph, PC6-Ur and PC10-Ur follow a similar trend where E_{ox}^{onset} is observed at more negative potentials affording a more destabilized HOMO in comparison to their phthalimide analogues. These findings align with the calculated trends from density functional theory (DFT) calculations [B3LYP/6-31+G(d)] using model compounds based on the repeat unit structures (PE-Ph and PE-Ur in Fig. S20 and Table S4, SI). Specifically, stabilization of the LUMO (PE-Ph/PE-Ur LUMO = −2.78/−1.07 eV) and a decrease in E_g (PE-Ph/PE-Ur E_g = −2.33/−4.04 eV) was observed and is consistent with similar compounds from literature reports.[41]

Next, increases in the peak anodic current/peak cathodic current (i_{pa}/i_{pc}) as a function of scan rate (25–300 mV s^{-1}) were measured for PC6-Ph, PC6-Ur, PC10-Ph, and PC10-Ur (Fig. S21 with the quantitative data compiled in Tables S5–S8, SI). A linear and comparable increase in i_{pa}/i_{pc} with an increasing voltage scan rate was observed indicating that electrochemical oxidation is reversible and not diffusion limited.[55–57]

Thermal analysis

Analysis of the polymer thermal properties was performed using thermogravimetric analysis (TGA) and differential scanning calorimetry (DSC) with the findings provided in Fig. 2B, Table 1, and Fig. S17. TGA indicates decomposition temperatures (T_d at 5% mass loss) within a proximal range of 292–320 °C highlighting the polymers' excellent thermal stability up to ~300 °C and comparable to ProDOT copolymers with *N*-containing functionalities (Table 1).[58] The thermograms also show notable mass loss events during pyrolysis that could correspond to alkyl sidechain cleavage and functional group degradation (~300–400 °C) followed by degradation of the polymer backbone (~450–500 °C), which has been reported for functionalized polythiophenes and various polymers.[59,60] DSC measurements show an absence of thermal transitions corresponding to polymer melt (T_m) or crystallization (T_c) indicating an amorphous morphology, which is expected for these polymers given the regiorandom incorporation of the Ph or Ur functionalities on the EDOT comonomer. Note, regiorandom incorporation of the phthalimide or urea substituent could inhibit formation of the periodic microstructure and self-assembly necessary to achieve semicrystalline domains.

MALDI-TOF analysis

MALDI-TOF spectrometry was used to determine the molecular weight distribution of the polymers, due to incompatibility with the GPC eluent and an absence of end-groups in the NMR spectra suitable for estimating M_n, with the results provided in Fig. 3 and S18 and Tables 1 and S3. MALDI-TOF was performed using polymer films drop-casted from CF solutions (0.25 mg mL^{-1}) with *trans*-2-[3-(4-*tert*-butylphenyl)-2-methyl-2-propenylidene]malononitrile (DCTB) as the matrix material, which has been successfully implemented as matrix material for ProDOT–EDOT copolymers and other polythiophenes.[61] Note, terthiophene was also evaluated as a matrix material, but the optimal ionization and signal intensity was achieved using DCTB.[62]

PC6-Ph provided *m*/*z* peaks corresponding to the desired repeat unit ranging from the trimer to the tetramer affording a M_n of 3.7 kg mol^{-1} and $Đ$ of 1.05 (Fig. 3). Although the M_n value is lower than many polythiophenes, this value is within range of other ProDOT–EDOT copolymers and polythiophenes with polar sidechains.[63,64] Additionally, it is possible that the higher-molecular polymer chains were not detected due to preferential ionization/detection of low molecular weight species.[65,66] End-groups for PC6-Ph were identified as containing both or combinations of Br and H (*e.g.* Br/Br, Br/H, and H/H) indicating dehalogenation as a likely side-reaction, which is a commonly encountered in DArP.

PC10-Ph (M_n = 3.0 kg mol^{-1} and $Đ$ = 1.02) shows a *m*/*z* peak corresponding to the trimer with H/H end groups, and interestingly polymer chains containing ProDOT homocoupling defects were detected. Note, while MALDI-TOF does not directly confirm connectivity, the *m*/*z* peaks align well with polymer chains containing an abundance of the ProDOT comonomer indicating defective homocouplings as a likely occurrence. Homocouplings of electron-rich thiophene monomers, such as 3,4-alkoxythiophenes, has been reported for DArP, supporting this structural assignment.[61]

For PC6-Ur (M_n = 3.6 kg mol^{-1} and $Đ$ = 1.08) and PC10-Ur (M_n = 3.2 kg mol^{-1} and $Đ$ = 1.03), *m*/*z* peaks corresponding to

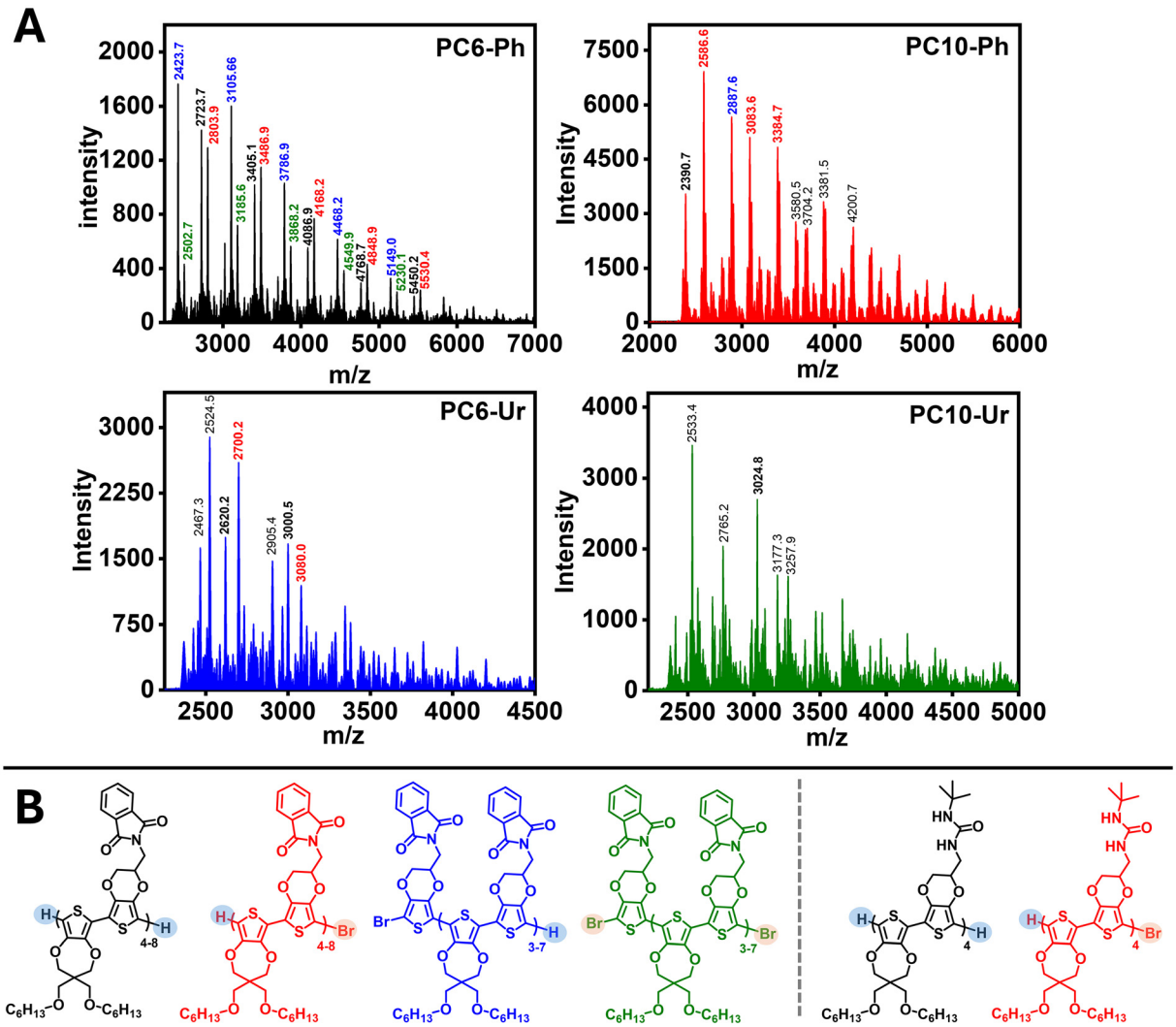

Fig. 3 (A) MALDI-TOF spectra of polymers PC6-Ph, PC10-Ph, PC6-Ur, and PC10-Ur. (B) Representative repeat units and end-groups for the ionized species detected *via* MALDI-TOF for PC6-Ph and PC6-Ur.

tetramers with H/H or H/Br end groups can be readily identified, but major intensity peaks likely correspond to polymers where matrix-adduct formation and subsequent fragmentation of the urea functionality is likely, since this has been reported with *N*-containing functional groups, such as urea, and the DCTB matrix (Fig. 3B).[67,68]

Electrochromic characterization

Spectroelectrochemistry and electrochromic switching measurements were performed using polymer coated glass-ITO substrates submerged in 0.5 M $LiPF_6$/PC electrolyte using a Ag/AgCl reference and a Ag-wire counter electrode. The spectroelectrochemical measurements and electrochromic switching dynamics are provided in Fig. 4 and the quantitative data compiled in Table 1. All films were electrochemically conditioned prior to measurement, as described above. It is acknowledged that film thickness and surface morphology play a critical role in determining the number of electrochemical redox accessible sites and the overall performance metrics for electrochromic conjugated polymers.[37] To account for this, proximal optical densities of ~0.8–1.1 were targeted for the optical absorption of the neutral polymer films, which is a typical range for solution processed electrochromic polymers.[39,69] For optical contrast ($\Delta T\%$), switching times (t_b/t_c), and cycling stability, the measured wavelength corresponds to λ_{max} of the neutral state (λ = 578, 541, 578, and 541 nm for PC6-Ph, PC6-Ur, PC10-Ph, and PC10-Ur respectively). Spectroelectrochemistry (Fig. 4A) indicates a dependence of the alkyl sidechain identity on the ProDOT comonomer (C6 or C10) on the potential needed to induce electrochromic switching and the optical absorption of the polaron. Specifically, with PC6-Ph/PC6-Ur marked bleaching of the ground state absorption band and growth of the p-polaron absorption band (~900–950 nm) occurs at more negative potentials (−1.2/−0.6 V) compared to PC10-Ph/PC10-Ur (−0.8/−0.4 V), respectively. However, complete bleaching of the ground state optical

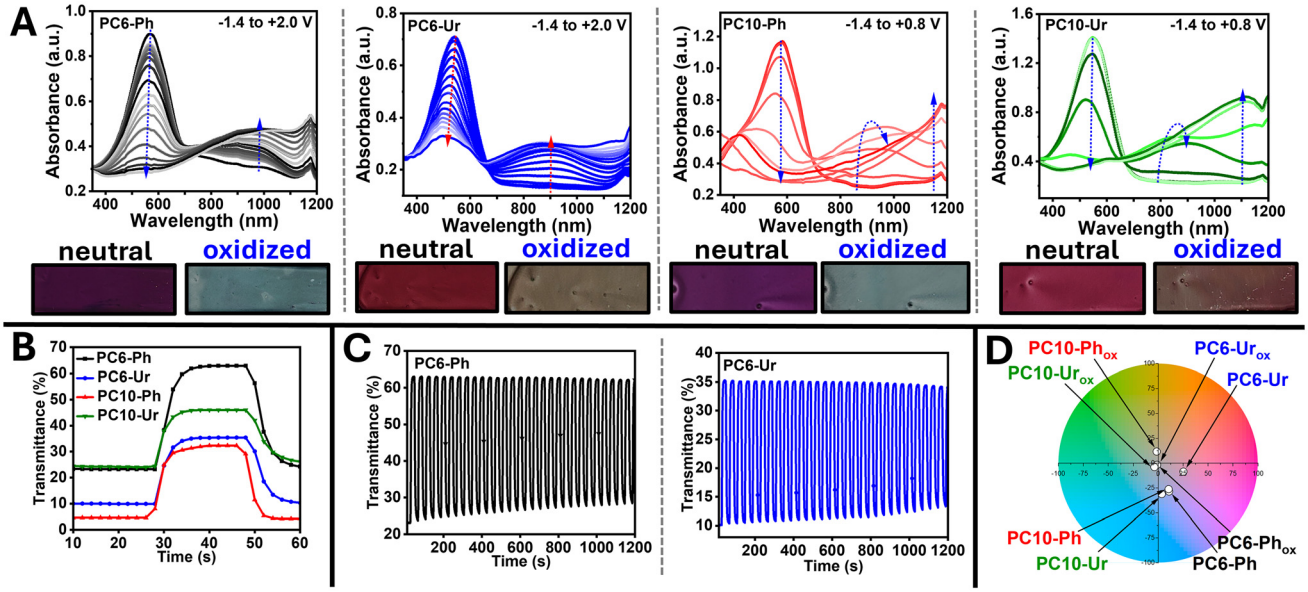

Fig. 4 Spectroelectrochemical spectra (A) and switching dynamics (B) of PC6-Ph, PC6-Ur, PC10-Ph, and PC10-Ur. (C) Representative cycling stability measurements of PC6-Ph and PC6-Ur. (D) CIELAB chromaticity diagram for neutral and oxidized PC6-Ph, PC6-Ur, PC10-Ph, and PC10-Ur.

absorption band occurs at lower potentials for PC10-Ph/PC10-Ur *versus* PC6-Ph/PC6-Ur (+0.6/+0.4 V *versus* +2.0/+2.0 V). Although the HOMO energy levels and E_{ox}^{onset} values are comparable for all polymers, the influence of the sidechain identity on the polymers morphology and microstructure may allow increased electrolyte penetration facilitating electrochemical oxidation at lower potentials. This is particularly apparent with the spectroelectrochemical spectra of PC6-Ur, which does not achieve complete bleaching of the ground state optical absorption band within the potential window of the electrolyte ($E_{ox} \leq +2.0$ V), indicating electrochemically inaccessible regions of the film. Lastly, for PC10-Ph/PC10-Ur an absorption band corresponding to the bipolaron becomes apparent at +0.2/+0.2 V. This contrasts with the optical absorption of the ground state (neutral form) where it was found the absorption profile is dependent on the phthalimide or urea functionality on the EDOT comonomer. It is likely that the influence of the ProDOT sidechain identity on the spectroelectrochemistry stems from the alkyl sidechain's role in the polymer self-assembly and microstructure, as well as influencing the electrolyte penetration and ion exchange under an applied bias.

Electrochromic optical contrast ($\Delta T\%$), switching times (t_b/t_c), coloration efficiencies [CE (η)], and cycling stability (Fig. 4B and C and Table 1) show dependence on both the identity of the alkyl substituent on ProDOT (C6 or C10) and the identity of the functional group on the EDOT monomers (phthalimide or urea). Specifically, PC6-Ph/PC6-Ur show comparable bleaching times (6.1/6.4 s), but the coloration time for PC6-Ur is sluggish compared PC6-Ph (15.2 *vs.* 10.4 s), which may be due to the urea functionality trapping electrolyte ions and inhibiting efficient exchange under negative potentials. Additionally, PC6-Ph affords an improved optical contrast compared to PC6-Ur ($\Delta T\%$ = 39.8 *versus* 28.9%) but a moderate coloration efficiency (CE = 55 *versus* 93 cm^2 C^{-1}). In comparison, PC10-Ph/PC10-Ur provide distinct performance metrics with more comparable optical contrast ($\Delta T\%$ = 27.7/32.3%) and coloration times (8.1/8.4 s). PC10-Ph shows very similar coloration efficiency to PC6-Ph (CE = 61 *versus* 55 cm^2 C^{-1}), indicating very little influence of the alkyl substituent identity for this metric, but a shorter switching time (t_b/t_c = 9.7/8.1 s *versus* 6.1/10.4 s). In comparison, PC10-Ur shows improved switching times (t_b/t_c = 6.2/8.4 s *versus* 6.4/15.2 s) but a diminished coloration efficiency (CE = 24.7 *versus* 93 cm^2 C^{-1}) relative to PC6-Ur. These findings emphasize the profound impact of the sidechain identity on the electrochromic performance metrics and reveal the nuanced relationship between the conjugated polymer sidechains and functional groups. The polymers all show comparable stability with minimal degradation after cycling for 1200 s (Fig. 4C and S23).

Changes in the coloration of PC6-Ph, PC6-Ur, PC10-Ph, and PC10-Ur following electrochromic switching are shown with CIE $L^*a^*b^*$ color coordinates provided in Fig. 4D and Table S9. The polymers PC6-Ph, PC6-Ph, PC10-Ph, and PC10-Ur all show a variable amaranth color in their neutral form. Upon electrochromic oxidation, all polymers achieve a transparent coloration. These findings show that by modification of the sidechain identity (C6 or C10) and the functional group (urea or phthalimide) the color of the polymer can be tuned to different shades of red/amaranth. It has been shown with ProDOT copolymers that the sidechain identity has a profound influence on the coloration, likely due to the influence of the sidechain identity on steric interactions and π-conjugation achieved through polymer backbone coplanarity.[30]

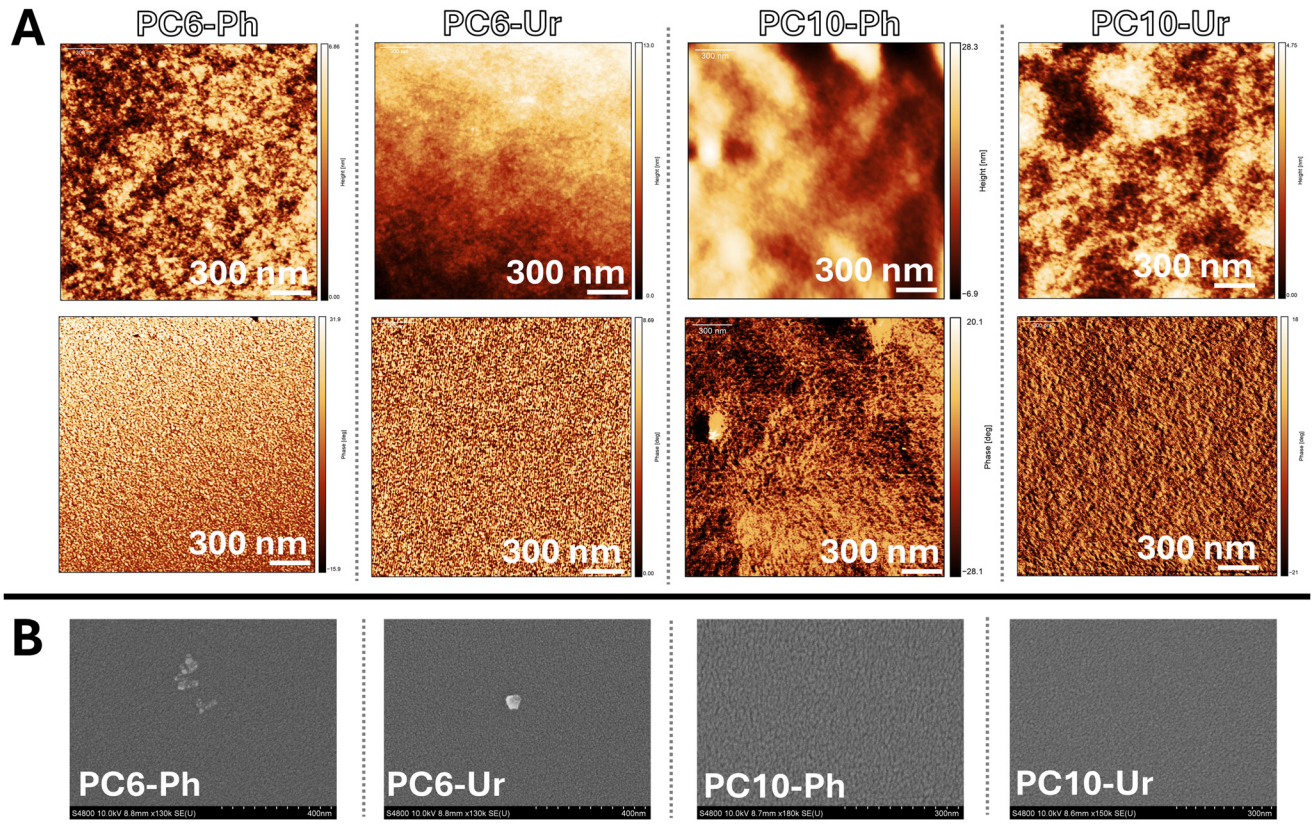

Fig. 5 AFM height (top) and phase (bottom) images (A) and SEM images (B) for PC6-Ph, PC6-Ur, PC10-Ph, and PC10-Ur.

Polymer morphology

AFM and SEM were employed to determine changes in the polymer morphology and surface topology due to modification of the ProDOT alkyl sidechain (C6 or C10) and the functionalization of the EDOT comonomer (phthalimide or urea). Polymer thin-films were prepared by spin-coating polymer/CF solutions onto glass substrates with the AFM height/phase images and SEM images provided in Fig. 5.[70] PC6-Ph, PC6-Ur, and PC10-Ur all show smooth, featureless morphologies in both AFM and SEM images with comparable RMS roughness (0.54, 0.51, and 0.51 nm, respectively). PC10-Ph also shows a comparable morphology but with an increased presence of polymer aggregates causing a steep increase in RMS roughness (3.85 nm). Correlating the surface topology of PC10-Ph to the electrochromic performance metrics, it is likely the presence of these aggregates results in the diminished optical contrast (25%), since the aggregates may inhibit electrolyte penetration thereby becoming electrochemically inaccessible. The smooth morphology of these polymers is characteristic of an amorphous morphology, which correlates well with DSC measurements that showed an absence of endothermic/exothermic transitions corresponding to a T_m/T_c. Additionally, these measurements show that the ProDOT sidechain identity (C6 or C10) and the functional group identity on EDOT (phthalimide or urea) hold minimal influence on the polymer morphology, which is likely due to the regiorandom arrangement of the functional groups on EDOT.

Conclusions

In this work, a series of ProDOT and EDOT copolymers were synthesized where the identity of the alkyl substituent on ProDOT [hexyloxy (C6) or decyloxy (C10)] and the functional group on EDOT [phthalimide (Ph) or urea (Ur)] was varied to probe how the alkyl substituent identity and inclusion of H-bonding functional groups influences the polymer optical, electrochemical, and electrochromic properties. The polymers, PC6-Ph, PC6-Ur, PC10-Ph, and PC10-Ur, were synthesized *via* direct arylation polymerization (DArP), which has been employed extensively for ProDOT/EDOT containing copolymers. Structural analysis *via* ATR-FTIR and NMR revealed incorporation of the desired functionalities from the monomer to the polymer. The polymer molecular weight distribution and end-group identity was analysed using MALDI-TOF spectrometry, which shows the presence of Br/Br, H/Br, and H/H end-groups indicating hydrodehalogenation as a likely side-reaction during the polymerization. In addition, MALDI-TOF spectrometry revealed the presence of ProDOT homocoupling defects for PC6-Ur, PC10-Ph, PC10-Ur, which

could not be realized using typical spectroscopic techniques (*e.g.* NMR). Electrochromic characterization shows the polymers have moderate optical contrasts (27.7–39.8%) and coloration efficiencies (up to 93 $cm^2\ C^{-1}$), albeit with more sluggish switching times compared to ProDOT/EDOT copolymers (t_b/t_c as low as 5.8/8.1 s). Regardless of the alkyl substituent identity, inclusion of the phthalimide functional group provides comparable switching times for PC6-Ph/PC10-Ph (t_b/t_c = 6.1/10.4 and 9.7/8.1 s) and coloration efficiencies (55 and 61 $cm^2\ C^{-1}$), while the urea functional group in PC6-Ur/PC10-Ur affords markedly different switching times (t_b/t_c = 6.4/15.2 and 6.2/8.4 s) and coloration efficiencies (93 and 25 $cm^2\ C^{-1}$) indicating greater dependence on the alkyl substituent identity, respectively. Lastly, DSC and AFM/SEM reveal an amorphous and featureless morphology for all the polymers, which is characteristic of regiorandom polythiophenes. Overall, these findings show that the identity of the alkyl substituent (C6 or C10) does not directly influence the polymer optical, electrochemical, or electrochromic properties, but is coupled with the identity of the phthalimide or urea functional group. It is foreseeable that inclusion of branched aliphatic sidechains or oligo(ethylene glycol) sidechains on the ProDOT comonomer could have more pronounced effects, as well as modification of the alkyl substituent on the urea, indicating areas for future research efforts.

Experimental

General

All reagents and chemicals were used as purchased from commercial sources: Fisher Scientific, VWR International, Sigma-Aldrich, and Ambeed Inc. All glassware for synthetic and characterization procedures was oven dried (120 °C) and cooled under N_2. Anhydrous propylene carbonate (PC) was purchased from Thermo Fisher Scientific, stored in a nitrogen-filled glovebox, and used as received. Glass-ITO substrates (Delta Technologies, Limited; RS = 15–25 Ω; 0.7 × 2.0 cm) were cleaned *via* sonication with an aqueous detergent, DI–H_2O, MeOH, isopropanol, and acetone (15 min) and UV-ozone treatment (20 min).

Polymer synthesis

An oven-dried 50 mL Schlenk tube with a stir bar was cooled under nitrogen. This was followed by the addition of 3 or 5 (0.23 mmol 1.0 equiv.) and 6 or 7 (0.23 mmol, 1.0 equiv.), PivOH (0.07 mmol, 0.3 equiv.), K_2CO_3 (0.58 mmol, 2.5 equiv.) and $Pd(OAc)_2$ (0.01 mmol, 0.04 equiv.) under nitrogen and vacuum-backfilled with N_2 three times. Then, 2.3 mL of anhydrous DMA was added to the mixture and stirred for 10 min at room temperature to dissolve the monomers. The Schlenk flask was then placed into a pre-heated oil bath (140 °C) for 24 h. After cooling at room temperature, polymer solids were dissolved in chloroform, and the reaction mixture was precipitated into the chilled hexanes with rapid stirring. The polymer product was then filtered into a cellulose thimble and purified *via* Soxhlet extraction (hexanes, MeOH, and chloroform). The chloroform fraction was concentrated and precipitated into chilled hexanes. The purple solid was then collected *via* filtration and dried overnight under vacuum.

MALDI-TOF analyses

A Bruker Microflex LRF MALDI-TOF mass spectrometer was used for measurements. The polymers were initially dissolved into $CHCl_3$ in the concentration of 1 mg mL^{-1}. Then the polymer solution was diluted on the concentration at 0.5 mg mL^{-1}. The matrix (DCTB) was prepared by dissolving into $CHCl_3$ in the concentration of 0.5 mg mL^{-1}, and it was combined with the polymer solution to yield a final concentration of 0.25 mg mL^{-1}. PEG 3500 was used as a calibration standard, and it was prepared by dissolving in $CHCl_3$ at 0.25 mg mL^{-1}. Number average molecular weights (M_n) and weight average molecular weights (M_w) were calculated following literature procedures.[61,71]

Cyclic voltammetry and optical absorption spectroscopy

A Shimadzu UV-3600 I Plus controlled by Lab Solutions software was used for all optical absorption measurements. Polymer films were prepared by spincoating (2500 rpm) 10 mg mL^{-1} $CHCl_3$ solutions (stirred at 65 °C overnight) onto 2 × 2 cm pre-cut glass-substrates. Cyclic voltammetry (CV) was performed using a BioLogic SP-50e potentiostat controlled by EC-Labs software. The working electrode was a glassy carbon electrode coated with a polymer film prepared *via* drop-casting from a 10 mg mL^{-1} $CHCl_3$ solution. Ag-wires served as the counter and pseudoreference electrodes, and all measurements were referenced to the Fc/Fc^+ redox couple. Degassed 0.1 M $LiPF_6$/PC served as the electrolyte, and all measurements were performed under an atmosphere of N_2. Prior to electrochemical analysis, the film was conditioned by cycling 10 times between −1.0 V to +1.0 V at a scan rate of 100 mV s^{-1}.

Electrochromic characterization

Spectroelectrochemisty and electrochromic switching measurements were performed using 0.5 M $LiPF_6$/PC electrolyte with a polymer coated glass-ITO substrate as the working electrode, a Ag-wire counter electrode, and a Ag/AgCl pellet electrode as the reference. Each polymer sample was dissolved in the concentration of 30 mg mL^{-1} in $CHCl_3$ and stirred overnight at 65 °C to ensure complete dissolution. Then, the polymer solution was spin-coated onto pre-cleaned glass-ITO substrates at 3000 rpm. The polymer films were electrochemically conditioned prior to measurement, as previously described. Optical transmittance was measured at the respective λ_{max} to determine optical contrast, switching times, coloration efficiency, and cycling stability.

Author contributions

Conceptualization: M. M. H. and R. M. P.; investigation, methodology and data acquisition and curation: M. M. H., R. S. R.,

K. S., M. S. M., A. M., A. B. R., M. L., S. T. S., Y. L., and R. M. P.; writing—original draft: M. M. H. and R. M. P.; writing—review and editing: M. M. H., R. S. R., K. S., M. S. M., A. M., A. B. R., M. L., S. T. S., Y. L., and R. M. P.; funding acquisition: R. M. P.

Conflicts of interest

There are no conflicts to declare.

Data availability

The data supporting the findings of this article have been included within the article and the supplementary information (SI). Supplementary information: monomer synthesis and characterization, polymer synthesis and characterization. See DOI: https://doi.org/10.1039/d5lp00413f.

Acknowledgements

M. M. H. and R. M. P. acknowledge support for this research by UT System STARS Program, UTEP University Research Institute, and UTEP Startup Awards. The authors acknowledge Prof. Katja Michael and Bryan Medina for their support in the MALDI-TOF measurements.

References

1 J. Mei and Z. Bao, *Chem. Mater.*, 2014, **26**, 604–615.
2 Y. Zhou, T. Kurosawa, W. Ma, Y. Guo, L. Fang, K. Vandewal, Y. Diao, C. Wang, Q. Yan, J. Reinspach, J. Mei, A. L. Appleton, G. I. Koleilat, Y. Gao, S. C. B. Mannsfeld, A. Salleo, H. Ade, D. Zhao and Z. Bao, *Adv. Mater.*, 2014, **26**, 3767–3772.
3 Y. He, N. A. Kukhta, A. Marks and C. K. Luscombe, *J. Mater. Chem. C*, 2022, **10**, 2314–2332.
4 J. Yao, C. Yu, Z. Liu, H. Luo, Y. Yang, G. Zhang and D. Zhang, *J. Am. Chem. Soc.*, 2016, **138**, 173–185.
5 X. Li, Y. Li, K. Sarang, J. Lutkenhaus and R. Verduzco, *Adv. Funct. Mater.*, 2021, **31**, 2009263.
6 Y. Yang, Z. Liu, G. Zhang, X. Zhang and D. Zhang, *Adv. Mater.*, 2019, **31**, 1903104.
7 N. Luo, P. Ren, Y. Feng, X. Shao, H.-L. Zhang and Z. Liu, *J. Phys. Chem. Lett.*, 2022, **13**, 1131–1146.
8 R. M. Pankow, B. Kerwin, Y. Cho, S. Jeong, G. Forti, B. Musolino, C. Yang, A. Facchetti and T. J. Marks, *Adv. Funct. Mater.*, 2023, **34**, 2309428.
9 B. Wei, L. Ouyang, J. Liu and D. C. Martin, *J. Mater. Chem. B*, 2015, **3**, 5028–5034.
10 A. L. Jones, M. De Keersmaecker, L. R. Savagian, B. T. DiTullio, I. Pelse and J. R. Reynolds, *Adv. Funct. Mater.*, 2021, **31**, 2102688.
11 J. F. Ponder, S. A. Gregory, A. Atassi, A. K. Menon, A. W. Lang, L. R. Savagian, J. R. Reynolds and S. K. Yee, *J. Am. Chem. Soc.*, 2022, **144**, 1351–1360.
12 Z. Bao, A. Dodabalapur and A. J. Lovinger, *Appl. Phys. Lett.*, 1996, **69**, 4108–4110.
13 I. McCulloch, M. Heeney, C. Bailey, K. Genevicius, I. MacDonald, M. Shkunov, D. Sparrowe, S. Tierney, R. Wagner, W. Zhang, M. L. Chabinyc, R. J. Kline, M. D. McGehee and M. F. Toney, *Nat. Mater.*, 2006, **5**, 328–333.
14 Z. Cao, L. Galuska, Z. Qian, S. Zhang, L. Huang, N. Prine, T. Li, Y. He, K. Hong and X. Gu, *Polym. Chem.*, 2020, **11**, 517–526.
15 H. You, D. Kim, H.-H. Cho, C. Lee, S. Chong, N. Y. Ahn, M. Seo, J. Kim, F. S. Kim and B. J. Kim, *Adv. Funct. Mater.*, 2018, **28**, 1803613.
16 Y.-H. Shih, G.-L. Chen, P.-H. Liu, K.-W. Tseng, W.-Y. Lee, W.-C. Chen, L. Wang and C.-C. Chueh, *ACS Appl. Electron. Mater.*, 2024, **6**, 1797–1808.
17 A. Giovannitti, C. B. Nielsen, D.-T. Sbircea, S. Inal, M. Donahue, M. R. Niazi, D. A. Hanifi, A. Amassian, G. G. Malliaras, J. Rivnay and I. McCulloch, *Nat. Commun.*, 2016, **7**, 13066.
18 J. Kim, R. M. Pankow, Y. Cho, I. D. Duplessis, F. Qin, D. Meli, R. Daso, D. Zheng, W. Huang, J. Rivnay, T. J. Marks and A. Facchetti, *Nat. Electron.*, 2024, **7**, 234–243.
19 Y. Yao, R. M. Pankow, W. Huang, C. Wu, L. Gao, Y. Cho, J. Chen, D. Zhang, S. Sharma, X. Liu, Y. Wang, B. Peng, S. Chung, K. Cho, S. Fabiano, Z. Ye, J. Ping, T. J. Marks and A. Facchetti, *Proc. Natl. Acad. Sci. U. S. A.*, 2025, **122**, e2414879122.
20 C. G. Bischak, L. Q. Flagg, K. Yan, T. Rehman, D. W. Davies, R. J. Quezada, J. W. Onorato, C. K. Luscombe, Y. Diao, C.-Z. Li and D. S. Ginger, *J. Am. Chem. Soc.*, 2020, **142**, 7434–7442.
21 Q. Wan, S. Seo, S.-W. Lee, J. Lee, H. Jeon, T.-S. Kim, B. J. Kim and B. C. Thompson, *J. Am. Chem. Soc.*, 2023, **145**, 11914–11920.
22 J. Y. Oh, S. Rondeau-Gagné, Y.-C. Chiu, A. Chortos, F. Lissel, G.-J. N. Wang, B. C. Schroeder, T. Kurosawa, J. Lopez, T. Katsumata, J. Xu, C. Zhu, X. Gu, W.-G. Bae, Y. Kim, L. Jin, J. W. Chung, J. B.-H. Tok and Z. Bao, *Nature*, 2016, **539**, 411–415.
23 M. Y. Lee, S. Dharmapurikar, S. J. Lee, Y. Cho, C. Yang and J. H. Oh, *Chem. Mater.*, 2020, **32**, 1914–1924.
24 Y.-C. Lin, C.-K. Chen, Y.-C. Chiang, C.-C. Hung, M.-C. Fu, S. Inagaki, C.-C. Chueh, T. Higashihara and W.-C. Chen, *ACS Appl. Mater. Interfaces*, 2020, **12**, 33014–33027.
25 X. Wang, C. Xu, N. Xu, L. Jiang, Y. Wang, F. Ni, G. Zhang, X. Gu and L. Qiu, *Macromolecules*, 2023, **56**, 5369–5380.
26 X. Yu, C. Li, C. Gao, X. Zhang, G. Zhang and D. Zhang, *SmartMat*, 2021, **2**, 347–366.
27 Q. Zhang, J. Huang, K. Wang and W. Huang, *Adv. Mater.*, 2022, **34**, 2110639.
28 Q. Wan and B. C. Thompson, *Adv. Sci.*, 2024, **11**, 2305356.

29 C. M. Amb, J. A. Kerszulis, E. J. Thompson, A. L. Dyer and J. R. Reynolds, *Polym. Chem.*, 2011, **2**, 812–814.
30 P. M. Beaujuge and J. R. Reynolds, *Chem. Rev.*, 2010, **110**, 268–320.
31 S. Macher, M. Schott, M. Sassi, I. Facchinetti, R. Ruffo, G. Patriarca, L. Beverina, U. Posset, G. A. Giffin and P. Löbmann, *Adv. Funct. Mater.*, 2020, **30**, 1906254.
32 L. M. Campos, A. J. Mozer, S. Günes, C. Winder, H. Neugebauer, N. S. Sariciftci, B. C. Thompson, B. D. Reeves, C. R. G. Grenier and J. R. Reynolds, *Sol. Energy Mater. Sol. Cells*, 2006, **90**, 3531–3546.
33 L. R. Savagian, A. M. Österholm, J. F. Ponder Jr., K. J. Barth, J. Rivnay and J. R. Reynolds, *Adv. Mater.*, 2018, **30**, 1804647.
34 B. T. DiTullio, L. R. Savagian, O. Bardagot, M. De Keersmaecker, A. M. Österholm, N. Banerji and J. R. Reynolds, *J. Am. Chem. Soc.*, 2023, **145**, 122–134.
35 F. A. Bravo-Plascencia, M. P. Flores-Morales, A. Kuhn, G. Salinas and B. A. Frontana-Uribe, *J. Mater. Chem. A*, 2025, **13**, 27772–27793.
36 P. Das, R. Elizalde-Segovia, B. Zayat, C. Z. Salamat, G. Pace, K. Zhai, R. C. Vincent, B. S. Dunn, R. A. Segalman, S. H. Tolbert, S. R. Narayan and B. C. Thompson, *Chem. Mater.*, 2022, **34**, 2672–2686.
37 J. Padilla, A. M. Österholm, A. L. Dyer and J. R. Reynolds, *Sol. Energy Mater. Sol. Cells*, 2015, **140**, 54–60.
38 T. Zubair, R. S. Ramos, A. Morales and R. M. Pankow, *Polym. Chem.*, 2025, **16**, 1188–1196.
39 G. S. Collier, I. Pelse, A. M. Österholm and J. R. Reynolds, *Chem. Mater.*, 2018, **30**, 5161–5168.
40 K. Perera, Z. Yi, L. You, Z. Ke and J. Mei, *Polym. Chem.*, 2020, **11**, 508–516.
41 J. Liu, W. Hou, D. Tang, Y. Gao, S. Yao, L. Jiang, Z. Zhang, M. Ouyang and C. Zhang, *ACS Sustainable Chem. Eng.*, 2022, **10**, 15978–15986.
42 S. Gupta and A. Patra, *New J. Chem.*, 2020, **44**, 6883–6888.
43 W. Zhang, R. Jamal, R. Zhang, Z. Yu, Y. Yan, Y. Liu, Y. Ge and T. Abdiryim, *Phys. Chem. Chem. Phys.*, 2020, **22**, 3592–3603.
44 D. Hu, B. Lu, X. Duan, J. Xu, L. Zhang, K. Zhang, S. Zhang and S. Zhen, *RSC Adv.*, 2014, **4**, 35597–35608.
45 P. Sitarik, S. S. Nagane, S. Chhatre, Y. Wu, Q. Baugh and D. C. Martin, *Mater. Adv.*, 2022, **3**, 6037–6049.
46 L. Ye, R. M. Pankow, M. Horikawa, E. L. Melenbrink, K. Liu and B. C. Thompson, *Macromolecules*, 2019, **52**, 9383–9388.
47 Y. Mu, Q. Sun and X. Wan, *RSC Appl. Polym.*, 2023, **1**, 190–203.
48 B. P. Charron, M. U. Ocheje, M. Selivanova, A. D. Hendsbee, Y. Li and S. Rondeau-Gagné, *J. Mater. Chem. C*, 2018, **6**, 12070–12078.
49 Y. Hao, G. Zhu and B. Li, *Ind. Eng. Chem. Res.*, 2024, **63**, 19350–19358.
50 J. F. Ponder Jr., A. M. Österholm and J. R. Reynolds, *Macromolecules*, 2016, **49**, 2106–2111.
51 A. M. Österholm, J. F. Ponder Jr., M. De Keersmaecker, D. E. Shen and J. R. Reynolds, *Chem. Mater.*, 2019, **31**, 2971–2982.
52 A. A. Advincula, A. L. Jones, K. J. Thorley, A. M. Österholm, J. F. Ponder and J. R. Reynolds, *Chem. Mater.*, 2022, **34**, 4633–4645.
53 K.-Y. Law, *J. Phys. Chem. Lett.*, 2014, **5**, 686–688.
54 T. Nicolini, J. Surgailis, A. Savva, A. D. Scaccabarozzi, R. Nakar, D. Thuau, G. Wantz, L. J. Richter, O. Dautel, G. Hadziioannou and N. Stingelin, *Adv. Mater.*, 2021, **33**, 2005723.
55 G. Sönmez, I. Schwendeman, P. Schottland, K. Zong and J. R. Reynolds, *Macromolecules*, 2003, **36**, 639–647.
56 H. Yu, S. Shao, L. Yan, H. Meng, Y. He, C. Yao, P. Xu, X. Zhang, W. Hu and W. Huang, *J. Mater. Chem. C*, 2016, **4**, 2269–2273.
57 R. S. Ramos, F. Muñoz-Alba, K. Saini, K. M. Castaneda, V. F. Juarez-Rangel, S. T. Sreenivasan, M. C. Ruiz Delgado, R. Ponce Ortiz and R. M. Pankow, *J. Mater. Chem. C*, 2025, **13**, 12772–12782.
58 A.-E. Bejan, C.-P. Constantin and M.-D. Damaceanu (Iosip), *J. Power Sources*, 2024, **613**, 234829.
59 S. Y. Son, G. Lee, H. Wang, S. Samson, Q. Wei, Y. Zhu and W. You, *Nat. Commun.*, 2022, **13**, 2739.
60 K. Pielichowski, J. Njuguna and T. M. Majka, in *Thermal Degradation of Polymeric Materials*, ed. K. Pielichowski, J. Njuguna and T. M. Majka, Elsevier, 2nd edn, 2023, pp. 49–147.
61 A. L. Jones, M. De Keersmaecker, I. Pelse and J. R. Reynolds, *Macromolecules*, 2020, **53**, 7253–7262.
62 A. E. Rudenko, A. A. Latif and B. C. Thompson, *J. Polym. Sci., Part A: Polym. Chem.*, 2015, **53**, 1492–1499.
63 H. Zhao, C.-Y. Liu, S.-C. Luo, B. Zhu, T.-H. Wang, H.-F. Hsu and H. Yu, *Macromolecules*, 2012, **45**, 7783–7790.
64 B. Ding, V. Le, H. Yu, G. Wu, A. V. Marsh, E. Gutiérrez-Fernández, N. Ramos, M. Rimmele, J. Martín, J. Nelson, A. F. Paterson and M. Heeney, *Adv. Electron. Mater.*, 2024, **10**, 2300580.
65 J. Vanderspikken, P. Verstappen and W. Maes, *Macromolecules*, 2024, **57**, 7138–7155.
66 M. Jayakannan, J. L. J. van Dongen and R. A. J. Janssen, *Macromolecules*, 2001, **34**, 5386–5393.
67 Y. Li, J. N. Hoskins, S. G. Sreerama and S. M. Grayson, *Macromolecules*, 2010, **43**, 6225–6228.
68 E. Altuntaş, K. Knop, L. Tauhardt, K. Kempe, A. C. Crecelius, M. Jäger, M. D. Hager and U. S. Schubert, *J. Mass Spectrom.*, 2012, **47**, 105–114.
69 G. S. Collier, R. Wilkins, A. L. Tomlinson and J. R. Reynolds, *Macromolecules*, 2021, **54**, 1677–1692.
70 M. S. Mahmud, A. Delgadillo, J. E. M. Urbay, M. S. Hassan, S. Zaman, D. Dieguez, D. Fontes, D. Leyva, J. Dantzler, A. Lopez, S. N. Joyce, D. A. Roberson, K. Michael, Y. Lin, A. N. Marchi and B. E. Schuster, *Polymer Degradation and Stability*, 2025, **232**, 111151.
71 C. Wesdemiotis, K. N. Williams-Pavlantos, A. R. Keating, A. S. McGee and C. Bochenek, *Mass Spectrom. Rev.*, 2024, **43**, 427–476.